International Journal of Electrochemical Science 20 (2025) 101128

Contents lists available at ScienceDirect

International Journal of Electrochemical Science

journal homepage: www.editorialmanager.com/ijoes

Development of a porous 304L Stainless steel substrate enhanced with graphene and platinum for hydrogen mitigation in passive autocatalytic recombiners

L. De Micheli *, G. Silvestrin, R.F.B. de Souza, A. Oliveira Neto, C. Giovedi

Instituto de Pesquisas Energéticas e Nucleares, Cidade Universitária, São Paulo, SP 05508-000, Brazil

ARTICLE INFO

Keywords:
Passive autocatalytic recombiners
Hydrogen safety
Graphene coating
Platinum doping
Hydrogen mitigation

ABSTRACT

The rapid expansion of the hydrogen economy poses significant safety challenges related to hydrogen handling across a wide range of applications. This study investigates the feasibility of using porous sintered 304 L stainless steel, coated with graphene and doped with platinum, as an advanced material for passive autocatalytic recombiners (PARs) to mitigate hydrogen release and improve operational safety. Detailed characterization using scanning electron microscopy (SEM), X-ray diffraction (XRD), and Raman spectroscopy confirmed the uniform deposition of graphene and platinum layers, as well as structural features such as spinel phase segregation. The low surface wettability, attributed to the armchair configuration of graphene edges, further enhances the material's suitability for catalytic recombination reactions in humid environments. Hydrogen removal tests demonstrated that an optimized platinum doping level of 0.5 wt% combined with a controlled substrate porosity of 50 μm resulted in a maximum hydrogen conversion efficiency of 40 %. These results highlight the critical influence of doping concentration and pore architecture on catalytic performance and overall PAR efficiency. Overall, this research provides valuable insights into the development of high-performance, passive hydrogen recombination systems, offering a promising pathway to improve safety and sustainability in emerging hydrogen technologies and to advance the hydrogen industry.

1. Introduction

Hydrogen is widely regarded as a promising clean energy carrier due to its high energy density and its potential to decarbonize various industrial and transportation sectors. However, the widespread implementation of hydrogen technologies still faces significant challenges, particularly regarding sustainable hydrogen production from water through electrolysis and related methods [1,2]. Producing hydrogen from water requires efficient and durable materials that can catalyze hydrogen evolution and recombination reactions while minimizing energy losses and operational risks. In this context, developing advanced materials for passive autocatalytic recombiners (PARs) plays a vital role in ensuring safety and efficiency in hydrogen handling and storage.

The hydrogen economy has emerged as a promising component of the global energy transition, providing a low-environmental-impact alternative to fossil fuels and playing a pivotal role in reducing greenhouse gas emissions [3]. As a clean energy carrier, hydrogen holds significant potential for broad application across various sectors, including transportation, power generation, and industrial processes. However, large-scale adoption is hindered by substantial safety challenges related to its handling, as hydrogen's physical and chemical properties make it highly flammable and capable of forming explosive mixtures with air. Hydrogen-oxygen mixtures with concentrations between 6 % and 30 % by volume are particularly hazardous, posing a high explosion risk [4,5]. Additionally, hydrogen-induced metal embrittlement can compromise the structural integrity of storage and transportation infrastructure.

To ensure safety, hydrogen production facilities employ advanced apparatuses inherited from combustible gas control systems used in nuclear technology. These systems are designed to mitigate risks associated with hydrogen production and include methods such as pre-inertization, post-accident inertization, electric recombiners, passive autocatalytic recombiners (PARs), igniters, and fan-induced mixing [4,6]. Among these, PARs stand out as a promising technology, utilizing passive catalytic recombination of hydrogen with oxygen in air.

PARs activate automatically as hydrogen concentrations rise, leveraging ambient oxygen for the recombination process. These devices

* Corresponding author.
E-mail address: lorenzo.demicheli@gmail.com (L. De Micheli).

https://doi.org/10.1016/j.ijoes.2025.101128
Received 3 June 2025; Received in revised form 13 July 2025; Accepted 13 July 2025
Available online 14 July 2025

operate without external power, relying on natural convection driven by the heat generated from the exothermic reaction [3]. This heat also sustains the autocatalytic process, promoting the mixing of combustible gases within the containment area [6].

Platinum and palladium are commonly used as catalysts in PARs due to their superior ability to adsorb hydrogen and oxygen. The exothermic recombination reaction on the catalyst surfaces generates convective flows, which aid in the dispersion of gases. However, the water vapor produced as a byproduct can diminish catalyst efficiency by inhibiting turnover, necessitating rapid water removal [7,8].

To mitigate water-induced deactivation, research has focused on hydrophobic materials. For instance, grafting perfluorooctyltriethoxysilane (FAS) onto traditional Pt-Al_2O_3 catalysts has demonstrated enhanced catalytic activity [9]. Graphene, known for its inherent hydrophobicity due to chain defects, presents another viable solution [8]. Recent advancements in plasma-based synthesis techniques, such as those using Tesla coil-generated plasma, have enabled the production of few-layer graphene flakes with controlled structural defects on various substrates, offering a scalable and cost-effective method for hydrophobic catalyst fabrication [10–12]. The graphene metal nanocomposites could offer superior hydrogen recombination performance under humid conditions, maintaining high catalytic activity and improved durability.

Moreover, stainless steel remains a practical and cost-effective substrate for passive recombiners due to its excellent thermal conductivity, mechanical strength, and corrosion resistance. New advances in porous sintered stainless steel have shown enhanced catalytic surface area and improved hydrogen recombination rates, supporting safer and more efficient operation in nuclear and industrial settings [13].

In addition, non-thermal plasma (NTP) technologies have gained attention as a green and controllable method to synthesize and functionalize graphene–metal catalysts. Recent reports have demonstrated that plasma-assisted deposition can improve the dispersion of metal nanoparticles on graphene, tailoring the catalytic surface for optimized hydrogen oxidation [14,15]. These methods also allow fine-tuning of surface defects, further enhancing hydrophobicity and resistance to deactivation in humid conditions [16].

Stainless-steel mesh electrodes coated with platinum have been extensively investigated as efficient electrocatalysts for the hydrogen evolution reaction (HER). In a recent study, Yuda [17] demonstrated that depositing platinum nanoparticles onto stainless-steel mesh (Pt/SSME) notably enhances their catalytic activity toward HER.

Nevertheless, existing systems face limitations, including insufficient conversion capacity at high hydrogen release rates and the potential for catalyst overheating, which could inadvertently ignite the gas mixture [13]. High heat dissipation, a characteristic of metallic catalysts, is essential for addressing these challenges.

Considering these recent developments, this study investigates the use of sintered porous 304 L stainless steel substrates, coated with hydrophobic graphene derivatives doped with varying platinum concentrations, as an innovative catalytic system for PARs. The findings aim to contribute to the current literature and improve combustible gas control technologies.

It is important to highlight that in this study, the electrochemical behavior of the material was evaluated indirectly through functional tests conducted under realistic operating conditions, including variations in temperature, pressure, and hydrogen concentration. Although standard electrochemical techniques were not employed, the system's performance provides a direct indication of its electrochemical properties in a catalytic context. The developed porous 304 L stainless steel substrate, modified with graphene and platinum, plays a key role in enhancing the catalytic recombination of hydrogen and oxygen.

2. Experimental

To prepare the proposed catalytic materials for application in Passive Autocatalytic Recombiners (PARs), sintered porous metal filters made of 304 L stainless steel with a diameter of 28 mm and a thickness of 2.5 mm, featuring different pore sizes (5 μm, 20 μm, and 50 μm), were used as substrates. These substrates underwent a graphene deposition process using a non-thermal plasma generator [10] until a 2 % mass increase was achieved. Cyclohexane (Aldrich) served as the carbon precursor, and a 60 kV arc was applied with a flow of N_2(g) between a 316 L stainless steel electrode and the substrate. Post-deposition, the materials were washed with water and isopropyl alcohol and then dried. Platinum was then loaded onto the substrates in varying amounts: 0.25 %, 0.50 %, and 1.0 % by mass, by dispersing appropriate amounts of $H_2PtCl_6{\cdot}6H_2O$ (Aldrich) on the substrate surfaces. Platinum reduction and fixation were achieved using the Flash Joule Heating Method [12].

Characterization of the catalytic materials was conducted using Scanning Electron Microscopy (SEM) with a JSM-IT700HR (JEOL) equipped with a Schottky emission source. X-ray Diffraction (XRD) patterns were obtained using a Miniflex II diffractometer with Cu Kα radiation (wavelength 0.15406 Å) over a 2θ range of 2–90° at a scan speed of 2 min^{-1}. Raman spectra were collected with a Horiba Scientific MacroRam spectrometer equipped with a 785 nm laser, with 10 accumulations per spectrum and an exposure time of 30 s per acquisition. These settings were chosen to optimize the signal-to-noise ratio while minimizing sample degradation during measurement.

Contact angle measurements were performed according to ISO 15989/2004 using a KINO-SL150E goniometer. For each catalytic material, multiple measurements were taken on a minimum of five distinct samples, with ten readings per sample, and average values were recorded.

The crystalline phases present in the sintered stainless steel substrates and the deposited coatings were identified by matching the XRD patterns with standard reference cards from the ICDD Powder Diffraction File (PDF) database. The following cards were used for phase identification: austenite (γ-Fe, ICDD PDF #00-033-0397), martensite (α′-Fe, ICDD PDF #00-034-0529), $FeCr_2O_4$ spinel (ICDD PDF #00-022-0340), $Mn_{1.5}Cr_{1.5}O_4$ spinel (ICDD PDF #00-035-0782), Cr_2O_3 (ICDD PDF #00-038-1479), platinum (Pt, FCC, ICDD PDF #00-004-0802), and graphite (ICDD PDF #00-026-1076)

Hydrogen removal was measured in a reactor coupled to a residual gas mass analyzer. The setup consisted of a catalytic chamber with H_2 (20 ml min^{-1}) and O_2 (10 ml min^{-1}) flow and a chamber with a quadrupole mass spectrometer, DaQMS 200 M1, Prisma, Pfeiffer, equipped with a continuous dynode and Faraday cup detector with a sensitivity of 200 A $mbar^{-1}$. The chamber was evacuated with a turbomolecular pump assisted by a dry diaphragm pump (Hicube 80, Pfeiffer). The connection between the chambers was established through a gas dosing valve, enabling continuous H_2 detection at $m/z = 2$.

3. Results and discussion

Fig. 1 shows SEM images of sintered 304L stainless steel substrates coated with graphene and doped with platinum. The granular nature of the sintered stainless steel is evident, with grain size increasing as a function of the substrate's porosity. Graphene was uniformly deposited on the grains, forming micropoints that add a characteristic texture. Randomly distributed brighter spots represent deposited platinum, but no significant differences were observed in the amount of platinum added or the substrate's porosity.

To assess pore condition post-deposition, cross-sectional SEM images were taken (Fig. 2). The graphene and platinum deposits were significantly smaller than the pore sections, preventing clogging and allowing free gas flow through the porous structure, which is crucial for maintaining high catalytic efficiency.

Fig. 3 shows the XRD patterns of sintered 304L stainless steel substrates samples with varying porosities and platinum content. The XRD results revealed peaks corresponding to austenite (~41.9°, 51.8°, 75.4°) and martensite (44.3°, 65.1°, 83°) phases [13], as well as spinel phases

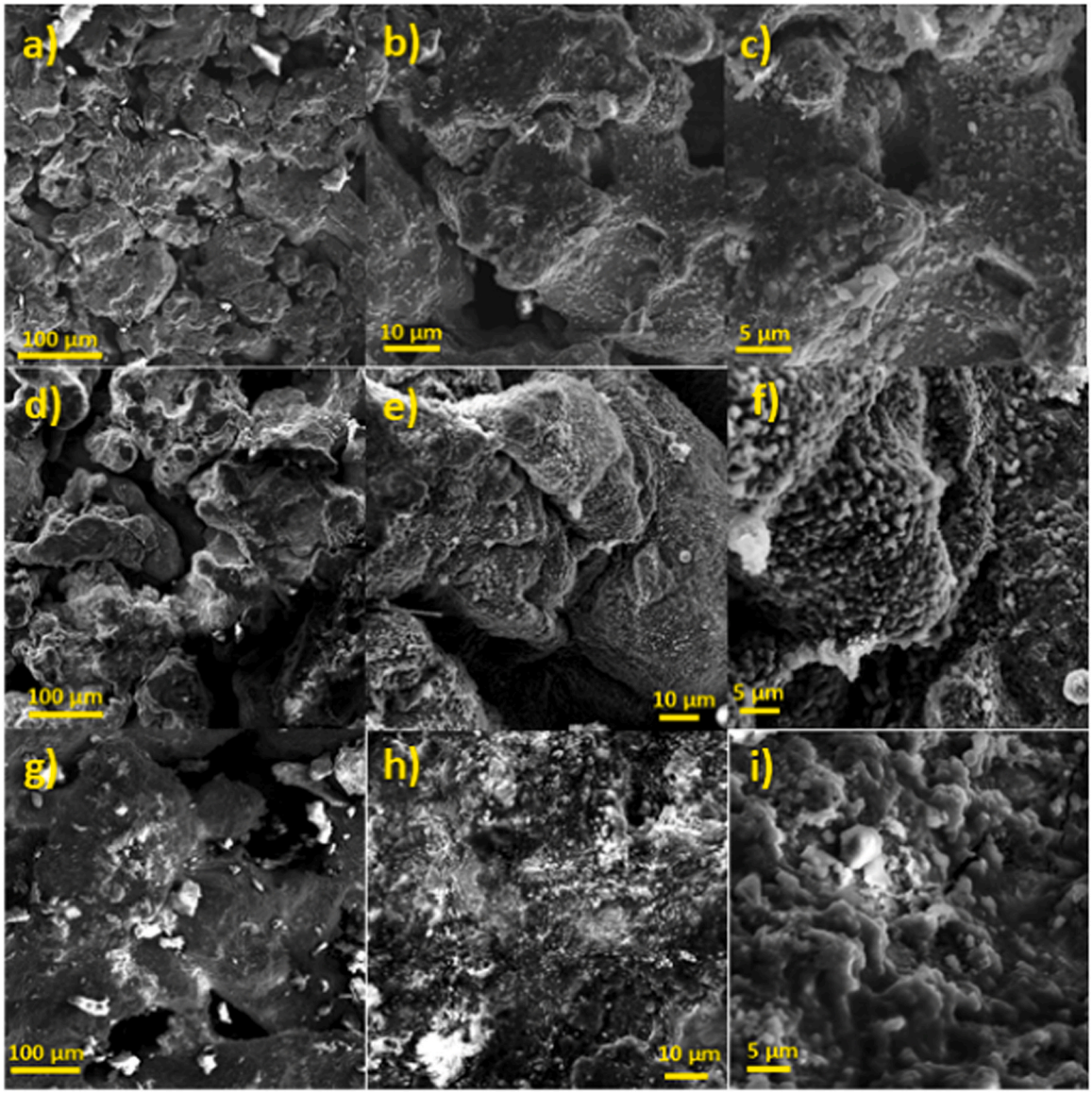

Fig. 1. SEM micrographs of sintered porous 304L stainless steel coated with graphene and doped with 0.50 % platinum on a substrate with pore sizes of a-c) 5 µm, d-f) 20 µm, and g-i) 50 µm at different magnifications.

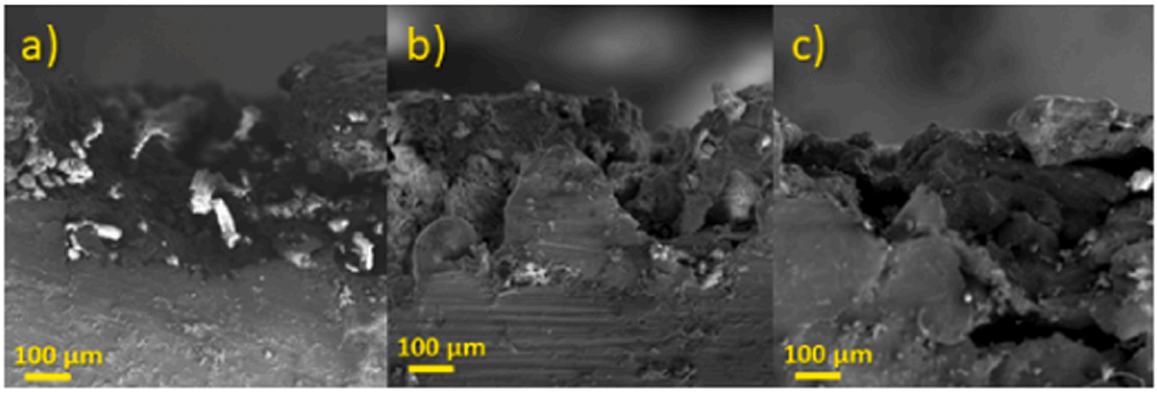

Fig. 2. SEM micrographs of cross-section sintered porous 304 L stainless steel coated with graphene and doped with 0.50 % platinum on a substrate with pore sizes of a) 5 µm, b) 20 µm, and c) 50 µm.

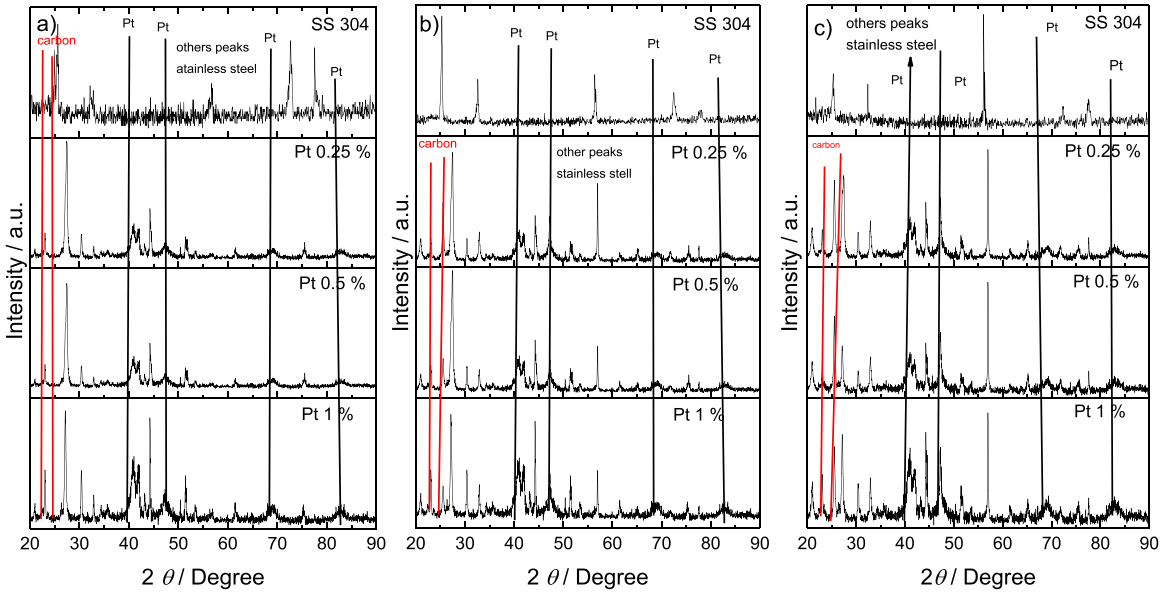

Fig. 3. XRD patterns of sintered porous metal substrates made from 304 L stainless steel (SS 304) coated with graphene and doped with platinum, showing different pore sizes: a) 5 μm, b) 20 μm, and c) 50 μm.

($Mn_{1.5}Cr_{1.5}O_4$ and $FeCr_2O_4$) and Cr_2O_3 at ~16.7°, 30.3°, 35.8°, 56.7°, 61.5°, 71.9°, 72.3°, and 77.5°, which are commonly reported for this type of stainless steel. Notably, the intensity of these peaks increased after the noble metal deposition, a phenomenon also reported in stainless steel subjected to heat treatment above 1000 °C [17]. This increase in intensity may be associated with improved crystallinity, which can enhance the stability and durability of the electrode under operating conditions. Platinum was identified by its characteristic face-centered cubic peaks at ~40°, 47°, 67°, and 82° [14], while carbon was detected with peaks centered at 23.1°, 25.4°, and 34.4° [18].

Raman spectroscopy valuable information, such as the quality of graphene materials. In the Raman spectrum (Fig. 4), the characteristic peaks of graphene can be observed, corresponding to the D and G bands, centered at approximately ~ 1320 and ~ 1595 cm^{-1}, respectively [19]. Fig. 4 also shows the convolution of the D1, D2, D3, D4, and G bands, with peaks appearing in the lower frequency regions at ~1320, 1628, 1425, 1176, and 1593 cm^{-1} [20].

In the literature, it is well-established that the G band corresponds to the first-order scattering of the $E_{2\,g}$ mode, associated with sp^2carbon.

Table 1
Relations between Band D and Band G for different catalytic materials for PARs.

PtContent (m/m)	Porosity					
	5 μm		20 μm		50 μm	
	I_{D1}/IG	I_{D1}/I_{D2}	I_{D1}/IG	I_{D1}/I_{D2}	I_{D1}/IG	I_{D1}/I_{D2}
0.25 %	4.5	14.3	2.5	19.7	2.6	13.5
0.50 %	2.3	14.5	2.7	20.1	2.6	22.1
1.0 %	2.4	15.4	1.9	27.7	2.8	29.6

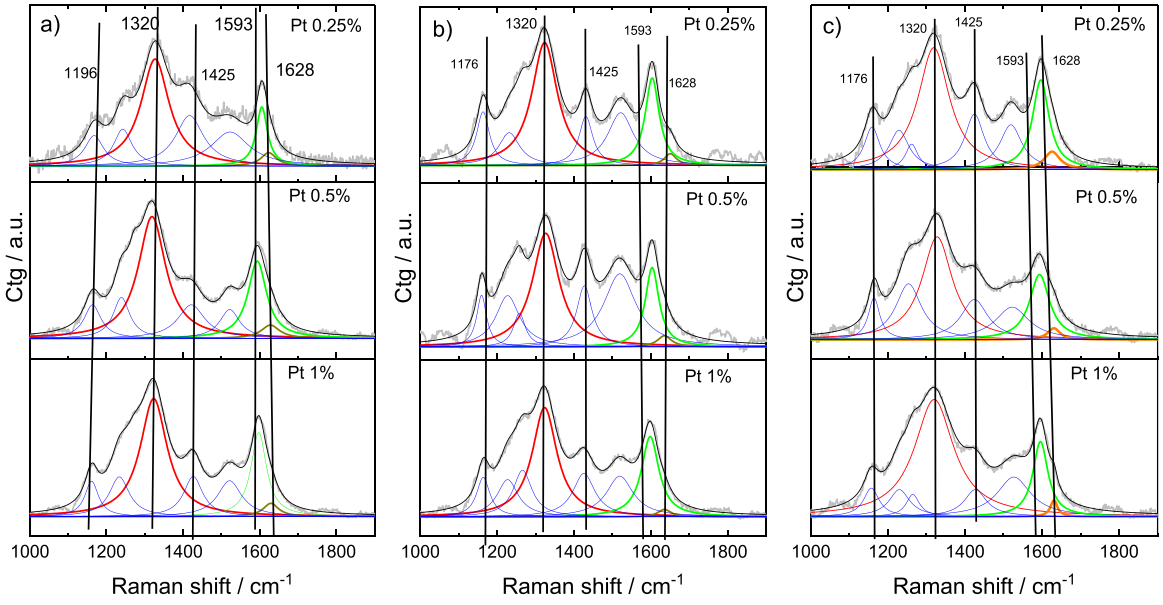

Fig. 4. Raman spectra of sintered porous metal substrates made from 304 L stainless steel coated with graphene and doped with platinum, showing different pore sizes: a) 5 μm, b) 20 μm, and c) 50 μm. The grey line represents the measured spectrum, the black line represents the modeled spectrum, the red line represents the D1 band, the green line represents the G band, the orange line represents the D2 band, and other bands are shown in blue.

The D band, on the other hand, is typically linked to structural defects, carbon amorphism, or edge defects that influence symmetry and selection rules [21]. A key parameter used to characterize the degree of disorder in graphene is the Raman intensity ratio between the D and G bands (I_{D1}/I_G) [19]. As shown in Table 1, the addition of platinum to the graphene material alters the D-to-G band ratio, indicating structural disorder within the carbon framework. This increase in disorder suggests a higher density of active sites, which is beneficial for catalytic reactions such as the hydrogen evolution reaction (HER). This may suggest that the material consists of nanosheets, similar to what has been observed in other graphene-based materials produced by the same process but on different substrates [11,12,22].

The ratio of I_{D2}/I_{D1} was used to further investigate the types of defects generated in the material. The data indicate a predominance of sp^3 hybridization defects, likely caused by the platinum addition. Such sp^3-type defects can further modulate the electronic structure of graphene, potentially enhancing the interaction between platinum nanoparticles and the carbon matrix, thereby improving catalytic activity and durability. These defects increase with higher platinum content, consistent with observations made for organometallic complexes by Day [23].

Graphene's hydrophobicity is closely related to its structure, including edge configuration and the presence of defects. Armchair-type edges tend to have more saturated carbon atoms than zigzag-type edges, and this greater saturation can have a significant effect on hydrophobicity [24]. From an application perspective, the balance between hydrophobicity and defect density must be optimized to ensure sufficient reactant access while maintaining good catalyst stability.

Overall, the combination of SEM, XRD, and Raman results indicates that the fabricated electrode possesses a porous structure with uniformly distributed catalytic sites, structural defects that enhance active surface area, and stable metal–support interactions.

To assess the hydrophobicity of the obtained materials, contact angle measurements were conducted on all prepared samples (Fig. 5). It was observed that the addition of graphene to the 304 L sintered stainless steel substrate increased the contact angle from 38.1° to 128°, indicating a low wettability material, which confirms the strong presence of armchair-type edges in the graphene. With the platinum doping, the contact angles slightly decreased to ~124°, which could be attributed either to water's affinity for platinum or to the sp^3 defects in the material. The contact angles for all prepared samples are presented in Table 2.

Hydrogen removal was measured by passing a constant flow of hydrogen and oxygen through the sintered porous metal substrates made from 304 L stainless steel coated with graphene and doped with platinum (Fig. 6). In this experiment, the removal was measured after the curve stabilized, and it was observed that the best results were obtained with 0.50 % platinum doping and a porosity of 50 μm, removing 39.9 % of the injected hydrogen—over five times more than the 0.25 % platinum doping on a 5 μm porous support. These results suggest an optimal combination of porosity and doping. Metal substrates with lower porosity exhibited lower activity, but this increased with a higher platinum concentration or larger pore size. This is likely related to the production and removal of water.

In our system, the hydrophobic nature of the graphene-coated surface plays a key functional role by preventing excessive accumulation of water or moisture on the catalyst's surface. Such water accumulation could otherwise block the active sites, hindering hydrogen adsorption and recombination reactions. By maintaining a more hydrophobic surface, the material helps ensure that liquid water does not persist on the catalyst, thus preserving the availability of catalytic sites for efficient hydrogen recombination.

Platinum acts as an active catalytic site for hydrogen oxidation and oxygen reduction, facilitating the surface reactions necessary for hydrogen mitigation. Graphene could contributes by improving the electrical conductivity and providing a high-surface-area support for the platinum particles, enhancing their dispersion and stability.

Table 2
Values of contact angles for different samples.

PtContent (m/m)	Porosity		
	5 μm Water contact angles / Degree	**20 μm** Water contact angles / Degree	**50 μm** Water contact angles / Degree
304 L SS	38.1 + /- 2.2	-	-
304 L graphene	128.6 + /- 4.2	129.2 + /- 2.2	128.6 + /- 4.4
0.25 %	122.8 + /- 5.2	124.1 + /- 2.9	123.1 + /- 4.3
0.50 %	124.2 + /- 4.1	123.6 + /- 3.4	123.6 + /- 4.5
1.0 %	127.3 + /- 6.1	129.2 + /- 5.3	125.0 + /- 2.6

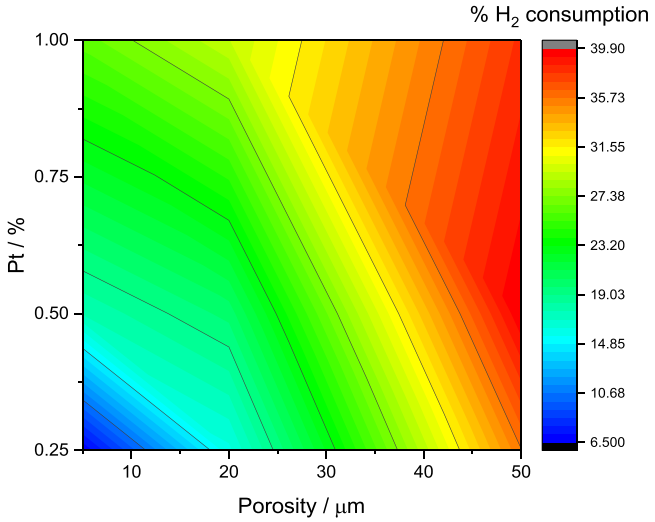

Fig. 6. % hydrogen removal in sintered porous metal substrates made from 304 L stainless steel coated with graphene and doped with platinum.

4. Conclusions

This study demonstrated the potential of sintered porous metal substrates made from 304 L stainless steel coated with graphene and doped with platinum for PAR applications. Characterization confirmed the homogeneity of graphene and platinum deposition, highlighting structural features such as spinel phase segregation. The material's low

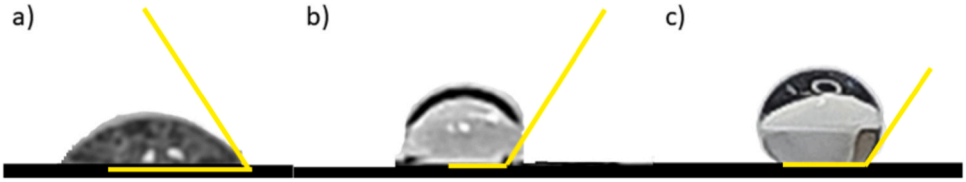

Fig. 5. Water contact angles of different samples: a) sintered porous 304 L stainless steel (porosity 5 μm), b) sintered porous 304 L stainless steel coated with graphene (porosity 5 μm), and c) sintered porous 304 L stainless steel coated with graphene, and 0.50 % Pt (porosity 5 μm).

wettability, attributed to the armchair structure of graphene edges, makes it suitable for PAR systems. The efficiency of hydrogen removal was significantly affected by the platinum doping and the porosity of the substrate. The best result was observed with 0.5 % platinum doping and 50 μm porosity, suggesting an ideal combination of porosity and doping, likely due to the amount of water produced and removed from within the pores. Therefore, while these results indicate potential benefits for enhancing passive autocatalytic recombination systems, they should be considered preliminary and limited to laboratory-scale static conditions. Further studies, including pilot-scale or real-world testing, are needed to validate the material's performance and durability under practical operating scenarios

Declaration of Competing Interest

The authors declare that they have no known competing financial interests or personal relationships that could have appeared to influence the work reported in this paper.

Acknowledgments

We are grateful to CAPES, CNPq (350514/2023-2, 302709/2020-7), and FDTE for financial supports.

References

[1] D.S. Nikitin, I.I. Shanenkov, P.M. Yeletsky, A. Nassyrbayev, R.B. Tabakaev, Y. L. Shanenkova, D.N. Ryskulov, A.I. Tsimmerman, A.A. Sivkov, Agricultural waste derived silicon carbide composite nanopowders as efficient coelectrocatalysts for water splitting, J. Clean. Prod. 442 (2024) 140890, https://doi.org/10.1016/j.jclepro.2024.140890.

[2] A. Sivkov, Y. Vympina, A. Ivashutenko, I. Rakhmatullin, Y. Shanenkova, D. Nikitin, I. Shanenkov, Plasma dynamic synthesis of highly defective fine titanium dioxide with tunable phase composition, Ceram. Int. 48 (8) (2022) 10862–10873, https://doi.org/10.1016/j.ceramint.2021.12.303.

[3] B. Gera, P.K. Sharma, R.K. Singh, K.K. Vaze, CFD analysis of passive autocatalytic recombiner, Sci. Technol. Nucl. Install. (2011) 1–9, https://doi.org/10.1155/2011/862812.

[4] M. Calabrese, M. Portarapillo, A. Di Nardo, V. Venezia, M. Turco, G. Luciani, et al., Hydrogen safety challenges: a comprehensive review on production, storage, transport, utilization, and CFD-based consequence and risk assessment, Energies 17 (2024) 1350, https://doi.org/10.3390/en17061350.

[5] L. Gardner, Z. Liang, T. Clouthier, R. MacCoy, A large-scale study on the effect of ambient conditions on hydrogen recombiner-induced ignition, Int. J. Hydrogen Energy 46 (2021) 12594–12604, https://doi.org/10.1016/j.ijhydene.2020.06.132.

[6] A.V. Avdeenkov, V.V. Sergeev, A.V. Stepanov, A.A. Malakhov, D.Y. Koshmanov, S. L. Soloviev, et al., Math hydrogen catalytic recombiner: Engineering model for dynamic full-scale calculations, Int. J. Hydrogen Energy 43 (2018) 23523–23537, https://doi.org/10.1016/j.ijhydene.2018.10.212.

[7] F. Morfin, J.C. Sabroux, A. Renouprez, Catalytic combustion of hydrogen for mitigating hydrogen risk in case of a severe accident in a nuclear power plant: study of catalysts poisoning in a representative atmosphere, Appl. Catal. B Environ. 47 (2004) 47–58, https://doi.org/10.1016/j.apcatb.2003.07.001.

[8] C. Xiao, Y. Yang, X. Zhou, Y. Du, Z. Tan, Humidity-tolerant H_2O_2 recombination platinum catalyst for mitigating hydrogen using silicalite-1 as support, Microporous Mesoporous Mater. 279 (2019) 395–399, https://doi.org/10.1016/j.micromeso.2019.01.026.

[9] W. Yu, J. Tao, X. Yu, S. Zhao, S.T. Tu, H. Liu, A microreactor with superhydrophobic Pt–Al_2O_3 catalyst coating concerning oxidation of hydrogen off-gas from fuel cell, Appl. Energy 185 (2017) 1233–1244, https://doi.org/10.1016/j.apenergy.2016.01.048.

[10] J.L. Fiorio, M.L. Gothe, E.C. Kohlrausch, M.L. Zardo, A.A. Tanaka, R.B. de Lima, et al., Nanoengineering of catalysts for enhanced hydrogen production, Hydrogen 3 (2022) 218–254, https://doi.org/10.3390/hydrogen3020014.

[11] P.V.R. Gomes, R.N. Bonifacio, B.P.G. Silva, J.C. Ferreira, R.F.B. de Souza, L. Otubo, et al., Graphene deposited on glass fiber using a non-thermal plasma system, Eng 4 (2023) 2100–2109, https://doi.org/10.3390/eng4030119.

[12] P.V.R. Gomes, N.F.B. Azeredo, L.M.S. Garcia, P.J. Zambiazi, G.R. Morselli, R. A. Ando, et al., Layered graphene/hexagonal boron nitride nanosheets (Gr/h-BNNs) applied to the CO_2 photoconversion into methanol, Appl. Mater. Today 29 (2022) 101605, https://doi.org/10.1016/j.apmt.2022.101605.

[13] E.V. Bezgodov, S.D. Pasyukov, M.V. Nikiforov, A.A. Tarakanov, I.A. Popov, D. L. Moshkin, et al., External and internal ignition of a hydrogen-air gas mixture induced by a recombiner, At. Energy 135 (2023) 97–106, https://doi.org/10.1007/s10512-024-01087-7.

[14] J. Nandenha, G. Silvestrin, L. Otubo L, D.A. Andrade, R.F.B. de Souza, E. Antolini, et al., Enhanced carbon monoxide tolerance of platinum nanoparticles synthesized through the Flash Joule Heating Method, Int. J. Electrochem. Sci. 19 (2024) 100585, https://doi.org/10.1016/j.ijoes.2024.100585.

[15] L.L. Santos, R.P. Cardoso, S.F. Brunatto, Direct correlation between martensitic transformation and incubation-acceleration transition in solution-treated AISI 304 austenitic stainless steel cavitation, Wear 462-463 (2020) 203522, https://doi.org/10.1016/j.wear.2020.203522.

[16] N. Karimi, F. Riffard, F. Rabaste, S. Perrier, R. Cueff, C. Issartel, et al., Characterization of the oxides formed at 1000°C on the AISI 304 stainless steel by X-ray diffraction and infrared spectroscopy, Appl. Surf. Sci. 254 (2008) 2292–2299, https://doi.org/10.1016/j.apsusc.2007.09.018.

[17] Y.P. Hardianto, N.A. Noorwali, S.S. Shah, M.M. Mohamed, S.A. Abbas, M. Ashraf, M.A. Aziz, Platinum/Stainless-Steel mesh electrode fabrication via chemically thermal reduction for efficient hydrogen evolution reaction, J. Electroanal. Chem. 975 (2024), https://doi.org/10.1016/j.jelechem.2024.118723.

[18] S.M. Lee, S.H. Lee, J.S. Roh, Analysis of activation process of carbon black based on structural parameters obtained by XRD analysis, Crystals 11 (2021) 153, https://doi.org/10.3390/cryst11020153.

[19] A.C. Ferrari, D.M. Basko, Raman spectroscopy as a versatile tool for studying the properties of graphene, Nat. Nanotechnol. 8 (2013) 235–246, https://doi.org/10.1038/nnano.2013.46.

[20] Z. Lu, C. Wang, X. Chen, M. Song, W. Xia, Effects of buffer gas on N-doped graphene in a non-thermal plasma process, Diam. Relat. Mater. 118 (2021) 108548, https://doi.org/10.1016/j.diamond.2021.108548.

[21] J.B. Wu, M.L. Lin, X. Cong, H.N. Liu, P.H. Tan, Raman spectroscopy of graphene-based materials and its applications in related devices, Chem. Soc. Rev. 47 (2018) 1822–1873, https://doi.org/10.1039/C6CS00915H.

[22] N.G.Pereira Filho, E.P. Soares, J.C. Ferreira, R.F.B. de Souza, D.A. Andrade, A. Oliveira Neto, Development of hydrophobic graphenoid layer on Portland cement for non-thermal plasma method, Diam. Relat. Mater. 148 (2024) 111499, https://doi.org/10.1016/j.diamond.2024.111499.

[23] C.S. Day, V.W. Day, A. Shaver, H.C. Clark, Variations in platinum-carbon(sp3) bond lengths. Crystal and molecular structure of (1,5-cyclooctadiene)(.eta.1-cyclopentadienyl)methylplatinum(II), Pt(1,5-C8H12)(.eta.1-C5H5)(CH3), Inorg. Chem. 20 (1981) 2188–2193, https://doi.org/10.1021/ic50221a049.

[24] L.M. Malard, M.A. Pimenta, G. Dresselhaus, M.S. Dresselhaus, Raman spectroscopy in graphene, Phys. Rep. 473 (2009) 51–87, https://doi.org/10.1016/j.physrep.2009.02.003.